‘

Master's Thesis in Graduate School of
Library, Information and Media Studies

Interactive Eye Aberration Correction for Holographic Near-Eye Display

March 2021

201921651

Kenta Yamamoto

Interactive Eye Aberration Correction for Holographic Near-Eye Display
ホログラフィックニアアイディスプレイにおけるインタラクティブな目の収差補正

Student No.: 201921651
氏名：山本　健太
Name: Kenta Yamamoto

Distortions of observed images have been a long-standing problem in near-eye displays. Although many correction methods for optical system-dependent aberrations have been proposed, the image distortions caused by eye aberrations have not been studied thoroughly. In addition to the problem, eye aberrations are individual specific. Therefore, a system capable of correcting the aberration irrespective of the individual is necessary. In this study, an aberration-correctable holographic near-eye display (HNED) is proposed that can be used to interactively compensate for image distortions caused by eye aberrations. For the compensation of aberrations, a propagation equation was formulated which includes eye aberrations in the HNED, and a GUI that enables a user to correct eye aberrations on their own was developed. In this system, the image displayed on the HNED is updated based on the correction coefficients specified by the user. Experiments on human subjects were conducted to verify the effectiveness of the proposed method. The results of the experiments indicate that the minimum identifiable size in the HNED can be reduced by the aberration correction using the interface, and especially this aberration correction method is useful for the visibility of low visual-acuity users.

Principal Academic Advisors: Yoichi OCHIAI
Secondary Academic Advisors: Makoto FUJISAWA

Interactive Eye Aberration Correction for Holographic Near-Eye Display

Kenta Yamamoto

Graduate School of Library, Information and Media Studies

University of Tsukuba

March 2021

Contents

List of Figures

Chapter 1

Introduction

1.1 Background

Near-eye display is an essential technology for realizing the virtual and/or augmented reality because it can provide new visual experiences. The beginning of the near-eye display was Sutherland's head-mounted display in the 1960s [1]. Since his work, various near-eye display technologies have been studied for decades. Behind the trend of such research is that liquid crystal displays have been mass-produced, prices have fallen, and high-resolution and small-sized ones have become easier to produce. With the distribution of liquid crystal displays and the maturity of display technology, near-eye displays that can withstand practical use have been being developed. In addition, the development of laser technology has made it possible to reduce the size of the laser light source and increase the output power. The prosperity of inexpensive and high-quality laser light sources has led to the realization of displays with rich color tones and wave optics-based displays that take advantage of the coherence of lasers. Especially, holographic near-eye display (HNED), which is based on holographic computation, is considered to be an essential technology to display high resolution and 3D images. Various methods of HNED have been proposed in the past few years for the advancement of holographic display technologies. To make HNED easy to use for more people, it is important to make the device customizable for each individual.

Owing to the characteristics of the optical design, the near-eye displays have different design considerations than those of conventional displays. For example, it is necessary to consider the characteristics of the human eye, which is considered as a type of the imaging optical system in which a group of lenses consisting of a cornea and crystalline lens forms the image on the retina. Aberrations are inherent in the eyes: myopia, hyperopia, and astigmatism are some common ones. These eye aberrations are often measured to correct eye distortions in daily life with eyeglasses and contact lenses. Although various measurement methods and correction methods have been proposed, discussions in the area of near-eye displays have not been sufficiently conducted. In fact, most existing near-eye displays are designed for normal eyes and cannot be used with eyeglasses. Such a design is not a problem for users who use contact lenses; however, it is problematic for users who have eye problems that require eyeglasses.

The problem of eye aberrations has not been explored fully in the context of several near-eye displays. Maimone et al. [2] treated aberrations caused by the eye and the near-eye display as one "black box" and examined the importance and feasibility of aberration correction in

HNED. Takaki et al. [3] studied the importance of aberration correction in a Maxwellian-type near-eye display and demonstrated the realization of the correction. These studies demonstrate only the results of aberration correction and do not provide a sufficient formulation of the eye aberration problem and aberration correction method. Kim et al. [4, 5] proposed a method for calculating the phase distribution on the spatial light modulator (SLM) with aberration correction by the ray tracing of the optical system including the eyes. However, previous studies have not demonstrated how a user could apply appropriate aberration correction.

1.2 Research Motivation

In order to see the image displayed on the near-eye display clearly without eyeglasses, the method of correcting eye aberrations is important. When correcting the user's aberration, it is necessary to find out how to provide the optimum correction for each user's aberration. There are two methods for correcting each user's aberrations: measurement-based correction and user-adjusted correction. Table 1.1 summarizes the pros/cons of the two methods. In this research, user-adjust correction is adopted, because this method requires only a small device and allows the user to make adjustments detailedly.

Table 1.1: Pros/Cons of measurement-based correction and user-adjusted correction.

	Pros	Cons
Measurement-based Correction	• Aberration correction is possible automatically. • It is possible to reflect the state of the eyes in real time.	• The device size becomes large because the measuring device and the display are integrated into one device. • The sensitivity of the device becomes higher because eye measurement is delicate.
User-adjusted Correction	• The device size is small. • The user can adjust the correction detailedly.	• The user may fail to adjust the correction. • The user may have to repeat the adjustment many times.

1.3 Proposal of This Research

In this study, an aberration-correctable HNED and a GUI which enables users to correct aberrations interactively are proposed. To evaluate the proposed aberration-correctable HNED, imaging simulations are performed and actual optical systems are developed. The proposed aberration correction system has several coefficients for aberration correction, and the user can adjust each coefficient via an interface while checking the displayed image directly (Fig. 1.1). To test the effectiveness of the interface, an experiment involving human subjects was performed. The subjects were required to perform a task similar to the visual acuity test, which was aimed to demonstrate the quantitative improvement in the vision after the correction. The experimental results demonstrated that aberration correction was effective and considering the aberrations of the human eye could improve the quality of the image in HNED.

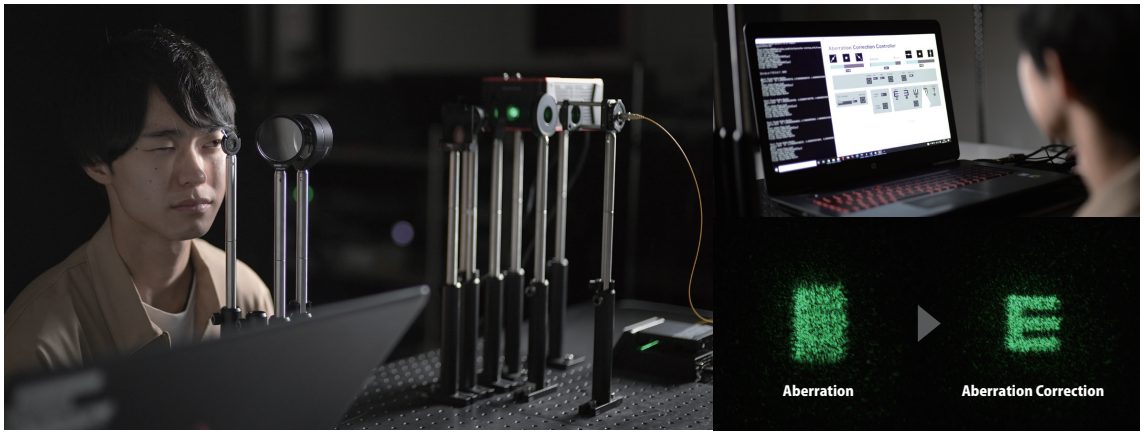

Figure 1.1: (left) Setup of proposed aberration-correctable holographic near-eye display and its user. (right above) The interface for aberration correction adjustment. (right below) The result of aberration correction that compensates distorted images.

1.4 Contributions

The main contributions of this study are the following:

- The propagation of light in the HNED including aberrated eyes was formulated and a calculating method for the phase distribution on the SLM was proposed that can compensate for the aberrations. A benchtop prototype of the HNED is also built.
- An interface that helps the users to correct aberrations interactively by themselves was developed.
- An experiment involving human subjects was performed to verify the effectiveness of aberration correction using the aberration-correctable benchtop prototype of the HNED and GUI.

Chapter 2

Related Work

2.1 Measurement, Correction, and Simulation of Eye Aberration

Correct visual information is important for humans to survive. Therefore, devices have been developed for those with poor or problematic eyesight. Technologies for the measurement and analysis of eye aberrations have been developed to quantify vision problems. For example, early studies on the measurement of vision were published more than two centuries ago, and the existence of spherical aberration in the human eye was recognized as early as in 1801 [6]. Subsequent studies have advanced our understanding of the human eye aberrations. These include the studies to measure the eye aberrations as a geometric aberration [7] and analyzing the aberrations using a subjective assessment [8, 9]. In contrast with these early methods, the wavefront aberration measurement using a Shack-Hartmann sensor led to a sudden improvement in the accuracy of the aberration measurement [10, 11, 12, 13]. This is an established method and has been incorporated into commercial aberration measurement products.

Along with establishing measurement methods, many aberration correction methods have also been developed. Eyeglasses are one of the most common methods of aberration correction. Because it is difficult to correct higher-order aberrations, a technology, such as contact lenses, capable of correcting such aberrations are required [14, 15, 16]. In addition to these two correction methods, various other methods of aberration correction have been proposed: using phase plates for aberration correction [17], incorporating adaptive optics to correct aberrations in real time while measuring eye aberrations [18], overlaying the compensation image with an optical see-through HMD [19], inserting intraocular lenses [20, 21], and corneal surgery using lasers [22].

Based on an improved understanding of the relationship between the aberration and visual field images, studies have been performed to simulate or experience how eye aberrations change the visual field image. Several methods, such as the point spread function (PSF) method [23, 24] and the rendering method [25, 26, 27, 28] have been used to simulate the visual field image with aberrations. As for the experienceable system for the aberrated visual field image, studies have used an optical system with built-in adaptive optics, called adaptive optics visual simulator (AOVS) that enables arbitrary aberrations to be delivered to the eye [29, 30, 31].

2.2 Vision-Correcting Display

People use displays naturally in their routines. This makes the comfort of viewing displays important for them. In the field of computational displays, a correction technique without eyeglasses for the visually impaired people has been developed. This technique is called "vision-correcting displays." An early method for computing the displayed image was proposed by Huang et al. [32]. Their method improves the visibility of the image by applying PSF to the displayed image, which is opposite to the aberration of the eyes. They also proposed a display method that achieves aberration correction by stacking multiple displays [33]. Later on, methods based on using light field displays for aberration correction have been proposed [34, 35].

2.3 Aberration Correction for Near-Eye Display

Image distortion due to aberration has been a problem in many near-eye displays. This problem is caused by optical system-dependent aberrations. Therefore, aberration correction methods have been considered [36, 37, 38, 39] to address this problem. Recent studies suggest that aberrations specific to optical systems can be compensated for by incorporating a camera into a feedback loop [40, 41].

Another important source of aberrations in near-eye displays is the human eye. Therefore, several studies have investigated eye aberrations in near-eye displays. Maimone et al. [2] considered both optical and eye aberrations together as a single aberration and described the feasibility and importance of aberration correction accordingly. Takaki et al. [3] described the effect of aberration in the Maxwellian-type near-eye display and presented the results of aberration correction. Although the aforementioned studies succeeded in demonstrating the results of aberration correction, they did not fully formulate the problem of eye aberration. Kim et al. [4, 5] defined the eye using a schematic eye model and established a method for calculating the phase distribution by adding aberration information to the ray tracing of the optical system including the eye. However, this method requires the precise shape of the eye of each user and cannot handle aberrations generally. Furthermore, there is no discussion on how users can actually adjust the aberration correction.

2.4 Position of This Study

In Table 2.1, the existing methods are summarized that offer displays that adapt to eye aberrations. These studies can be divided into two types: far-eye and near-eye display studies. Most existing methods of both types do not offer a deeper insight into how the user actually adjusts for the aberration correction, and no GUI for handling correction parameters has been proposed. Although there are methods with real-time aberration measurements, such as AOVS, it is difficult to incorporate them into a near-eye display because the miniaturization of these measurement systems is difficult. Therefore, a method for users to make their own corrections by providing a GUI is proposed in this thesis.

Table 2.1: Comparison with previous vision-correcting displays.

	Display Position	Display Type	GUI for User-defined Parameters	Real-time Aberration Measurement
Huang et al. (2011) [32]	Far-Eye	LCD	N/A	N/A
Fernandez et al. (2012) [29]	-	AOVS	N/A	Available
Pamplona et al. (2012) [34]	Far-Eye	Light Field Display	N/A	N/A
Huang et al. (2012, 2014) [33, 35]	Far-Eye	Light Field Display	N/A	N/A
Maimone et al. (2017) [2]	Near-Eye	Holographic Display	N/A	N/A
Takaki et al. (2018) [3]	Near-Eye	Holographic Display	N/A	N/A
Kim et al. (2019, 2020) [4, 5]	Near-Eye	Holographic Display	N/A	N/A
This Study	Near-Eye	Holographic Display	Available	N/A

Chapter 3

Principle

3.1 Light Propagation Formula in Wave Optics

HNED is a device that combines a near-eye display and a holographic projector [2]. This device can output images based on hologram calculations. Hologram computation is based on wave optics, which treats light as a wave and a point light source as a spherical wave; the computed hologram is called a computer-generated hologram [42].
A spherical wave is described by the following equation and is the basis of all hologram calculations:

$$\frac{1}{r}\exp(ikr) \tag{3.1}$$

where i is the imaginary number, k is the wavenumber, and r is the distance from the light source to the target position. In wave optics, the state of the light is expressed in complex amplitudes.
When dealing with the light propagation from one plane to another, one calculates the distribution of complex amplitudes on each plane. The source plane of the light propagation and the destination plane are defined as u_1 and u_2, respectively (Fig. 3.1). It is considered that the propagation of light between planes is composed of spherical waves generated from each point of the source plane. The light propagation equation derived from this idea is the Sommerfeld diffraction equation:

$$u_2(x_2, y_2) = \frac{1}{i\lambda}\int u_1(x_1, y_1)\frac{\exp(ikr)}{r}\cos\theta \, dx_1 dy_1 \tag{3.2}$$

where λ is the wavelength and $\cos\theta$ is the inclination factor which changes the propagation intensity ratio according to the angle.
In this study, the Fresnel diffraction propagation equation is utilized to calculate the light propagation. The Fresnel diffraction propagation equation is derived by substituting the distance approximation equation into the Sommerfeld diffraction equation (Eq. 3.2). The introduced distance approximation is a Taylor expansion of the distance r, which is the following approximation:

$$r = z\sqrt{1 + \frac{(x_2 - x_1)^2 + (y_2 - y_1)^2}{z^2}} \tag{3.3}$$

$$\approx z + \frac{(x_2 - x_1)^2 + (y_2 - y_1)^2}{2z} - \frac{((x_2 - x_1)^2 + (y_2 - y_1)^2)^2}{8z^3} + \cdots \tag{3.4}$$

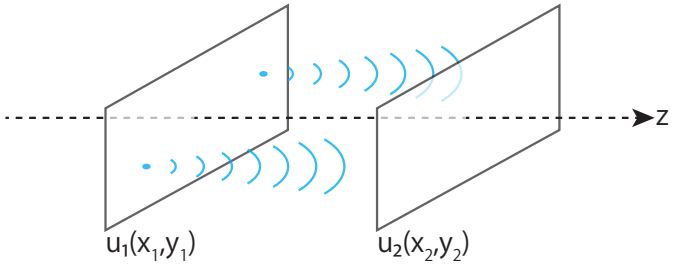

Figure 3.1: Light propagation from plane to plane. It is defined that spherical waves propagate from each point on the plane.

where z is the distance between the plane u_1 and the plane u_2 on the z-axis. When the third term is considered to be sufficiently smaller than the wavelength, the distance r is approximated by the following equation:

$$r \approx z + \frac{(x_2 - x_1)^2 + (y_2 - y_1)^2}{2z} \tag{3.5}$$

$$\lambda \gg \frac{((x_2 - x_1)^2 + (y_2 - y_1)^2)^2}{8z^3}. \tag{3.6}$$

By substituting this approximation into Eq. 3.2, the Fresnel diffraction propagation from u_1 to u_2 is represented by the following formula:

$$u_2(x_2, y_2) = \mathcal{F}^{-1}\left[\mathcal{F}\left[u_1(x_1, y_1)\right]\mathcal{F}\left[\exp\left(\frac{i\pi p^2}{\lambda z}\left(x_1^2 + y_1^2\right)\right)\right]\right] \tag{3.7}$$

where $\mathcal{F}$ is the Fourier transform, $\mathcal{F}^{-1}$ is the inverse Fourier transform, and p is the pitch size of the SLM. Because this equation is used many times in this thesis, it is defined as a function $Prop_z()$ as follows:

$$Prop_z(u_1(x_1, y_1)) = \mathcal{F}^{-1}\left[\mathcal{F}\left[u_1(x_1, y_1)\right]\mathcal{F}\left[\exp\left(\frac{i\pi p^2}{\lambda z}\left(x_1^2 + y_1^2\right)\right)\right]\right]. \tag{3.8}$$

3.2 Lens Imaging with Aberrations

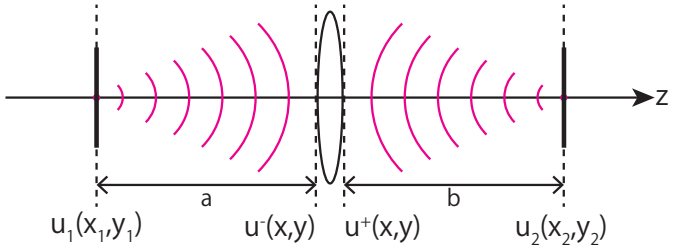

Figure 3.2: Convergence of a point light source by a lens.

In general, the role of the lens is to refocus a point light source (Fig. 3.2). It is known that the distance relationship between the point light source and the refocus point is represented by the following equation:

$$\frac{1}{a} + \frac{1}{b} = \frac{1}{f} \tag{3.9}$$

where a is the distance between the point light source and the lens, b is the distance between the lens and the refocus point, and f is the focal length of the lens. Utilizing Eq. 3.7 for the light propagation from the point light source to the focal point, the converging feature of the lens can be defined as the following phase distribution $t(x, y)$:

$$t(x,y) = \exp\left(-i\frac{\pi}{\lambda}\left(\frac{x^2+y^2}{f}\right)\right). \tag{3.10}$$

In such imaging optical systems, perceptible distortions occur owing to distortions by the lens. Such a distortion is defined as a wavefront aberration in wave optics. Wavefront aberration is a measure of the distance between the ideal and distorted wavefronts. Wavefront aberration is generally expressed using the Zernike polynomial as follows:

$$R_n^{\pm m}(r) = \sum_{s=0}^{\frac{(n-m)}{2}} \frac{(-1)^s (n-s)!}{s!(\frac{n+m}{2}-s)!(\frac{n-m}{2}-s)!}\ r^{n-2s} \tag{3.11}$$

$$Z_n^m(r,\theta) = \sqrt{2(n+1)}\ R_n^m(r) \begin{cases} \frac{1}{\sqrt{2}} & (m=0) \\ \cos|m|\theta & (m>0) \\ \sin|m|\theta & (m<0) \end{cases} \tag{3.12}$$

$$W(x,y) = \sum_{m=0}^{i}\sum_{n=0}^{j} \alpha_n^m Z_n^m(r,\theta) \tag{3.13}$$

where $R_n^{\pm m}(r)$ is the radial polynomial, $W(x, y)$ is the wavefront aberration, $Z_n^m(r, \theta)$ is the Zernike polynomial, and α_n^m is the Zernike coefficient.
Because these aberrations are caused by the lens, the aberrations must be considered in the lens equation. The aberration is included in the pupil function P and the generalized pupil function $\mathcal{P}$ is defined as follows:

$$\mathcal{P}(x,y) = P(x,y)\exp(ikW(x,y)). \tag{3.14}$$

Utilizing Eq. 3.10 and Eq. 3.14, the transformation equation for the complex amplitude distribution with an aberrant lens is defined as

$$u^+ = u^- * t(x,y) * \mathcal{P}(x,y) \tag{3.15}$$

where u^- and u^+ are the complex amplitude distributions at the front and behind the lens, respectively.
Figure 3.3 shows the simulation results based on Eq. 3.8 and Eq. 3.15 when parallel light is focused by a lens with aberration. It can be confirmed that the state of the focusing point (PSF) changes according to each aberration pattern.

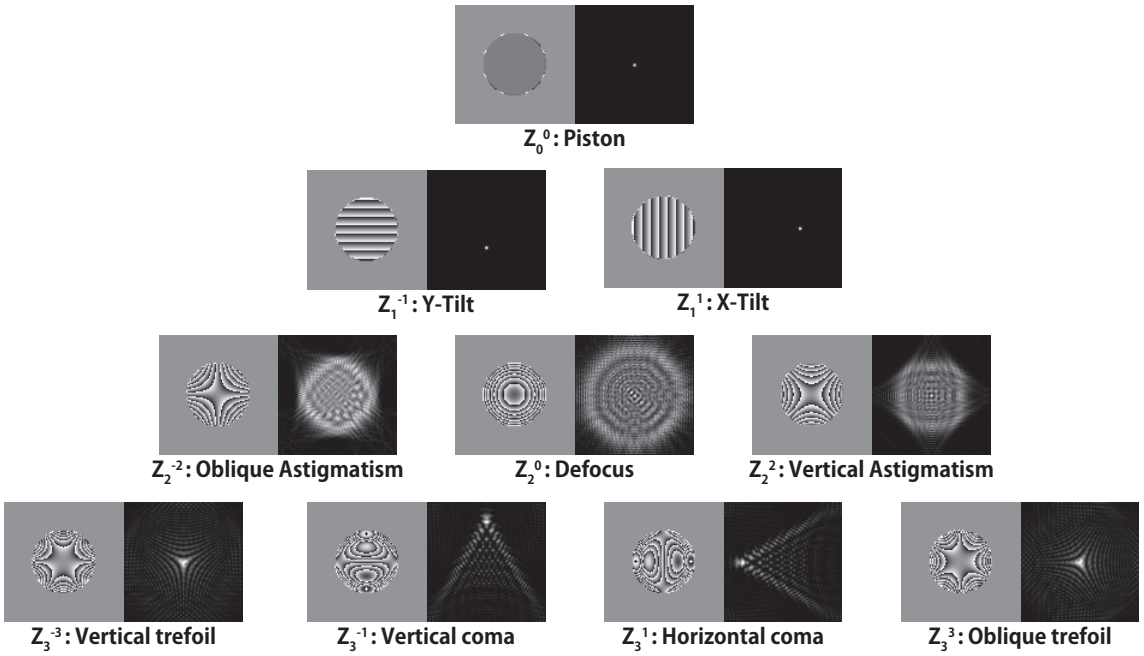

Figure 3.3: Each aberration of 10 kinds of Zernike polynomials. The image on the left is a map of the wavefront aberration, and the image on the right is the result of the convergence point of the lens with the wavefront aberration. The result of the convergence point (PSF) changes according to the characteristics of the aberration.

Chapter 4

Human Eye

4.1 Optics of Human Eye

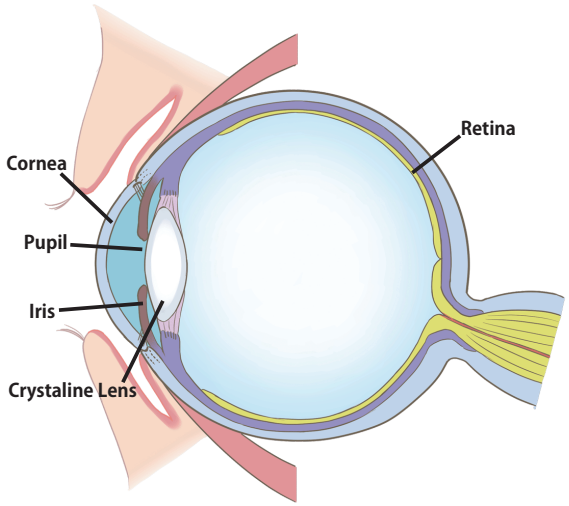

Figure 4.1: Anatomical sketch of the human eye.

The human eye is an optical imaging device. It consists of two lenses (the cornea and crystalline lens), an aperture (the pupil), and a sensor (the retina), as shown in Fig. 4.1. The cornea has a large curvature and contributes significantly to the refraction of light from the outside. The ciliary muscles are attached to the crystalline lens, and the focal length of the lens changes as the shape of the crystalline lens changes as the muscles shrink. The pupil plays an aperture role and is used to regulate the amount of light entering the eye. The retina is composed of rod cells and cone cells, and color information is transmitted to the brain through cells' reactions corresponding to wavelengths, similar to camera sensors. In this way, the human eye is a type of optical imaging system consisting of a lens and a sensor. The lens of the human eye has a similar distortion to the optical lens. For example, if the shape of the cornea is abnormal, the outside world's image cannot be properly imaged on the retina, and the eyesight deteriorates. In addition, cataracts, in which the crystalline lens becomes cloudy and visual acuity deteriorates, are also famous.

To properly deal with such eye abnormalities, it is necessary to know the eyes' condition accurately. Therefore measurement methods for eye aberrations have been developed to

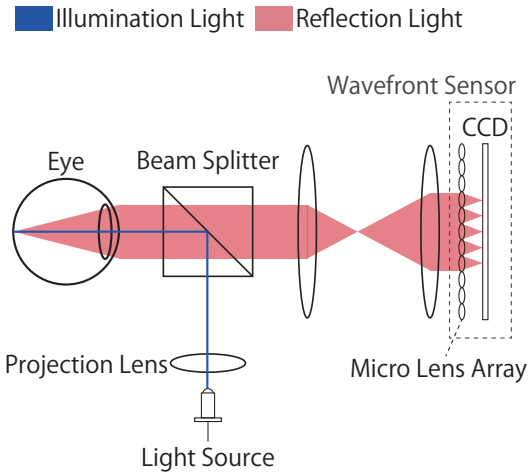

Figure 4.2: Schematic diagram of an optical system for measuring the wavefront aberration of the human eye.

quantify these aberrations optically. For example, there is a double-pass PSF method that analyzes the PSF that represents the optical state of the eye [43]. Because this method can directly measure the PSF of the eye, it is easy to apply to the simulation of how the visual field looks with aberration. However, the measurement steps are complicated and the component analysis of the aberration cannot be performed.

On the other hand, it is the method of measuring wavefront aberration that can easily analyze the aberration components and examine the eye's aberration information in detail [10, 11, 12, 13]. The basic configuration diagram of the measurement method is shown in Fig. 4.2. In the measurement, the entire eye is regarded as one optical system, and the cornea and the crystalline lens are regarded as one lens. In the measurement, an infrared laser beam (generally superluminescent diode is used) with a tiny beam diameter is incident on the eye. The incident light is diffusely reflected at the fundus and exits the eye through the crystalline lens and cornea. By passing through the eye's lens, the diffused light from the fundus is collimated and becomes parallel light. Wavefront aberration can be found by observing this parallel light with a sensor using a microlens array. In this study, as with the measurement method, the eye is regarded as one optical imaging system and treated as having one wavefront aberration.

4.2 Imaging Formula of Human Eye

In the previous section, the eye optics is defined as an optical imaging system consisting of a composite lens and a sensor. To make the eye's optical system simulable, the imaging optics of the eye based on the wave optical calculations is formulated. In the human eye without any refractive error, the focal length of the lens coincides with the distance to the retina when the eye is focused at infinity. When observing an object closer than the infinity, the focal length of the eye lens changes such that Eq. 3.9 holds. For example, when the distance from the eye to the object is a and the distance from the lens of the eye to the retina is b (depicted in Fig. 4.3), the image of the object on the retina is given by the following

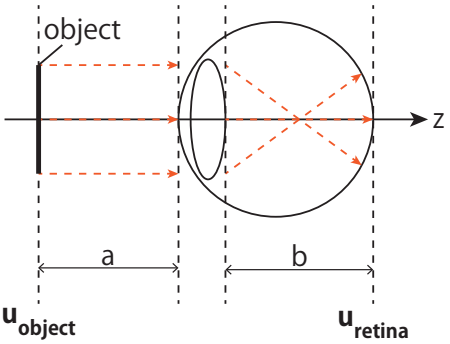

Figure 4.3: Schematic diagram of imaging onto the retina.

propagation equation:

$$u_{retina} = Prop_b\ (Prop_a(u_{object}) * t(x,y) * \mathcal{P}(x,y)). \tag{4.1}$$

Since the lens and the aberration of the lens is expressed by the equation of $t(x,y) * \mathcal{P}(x,y)$ ($\mathcal{P}(x,y)$ includes the wavefront aberration $W(x,y)$), it is possible to simulate the imaging process by the eye with aberration.

Chapter 5

Holographic Near-Eye Display

5.1 Optical Design of HNED

In recent years, various methods of HNED have been proposed. In this section, two HNED methods are formulated with reference to the method of Maimone et al. [2]. As shown in Fig. 5.1, there are two types of optical systems of HNED. These two types are classified according to whether or not the eyepiece is used.

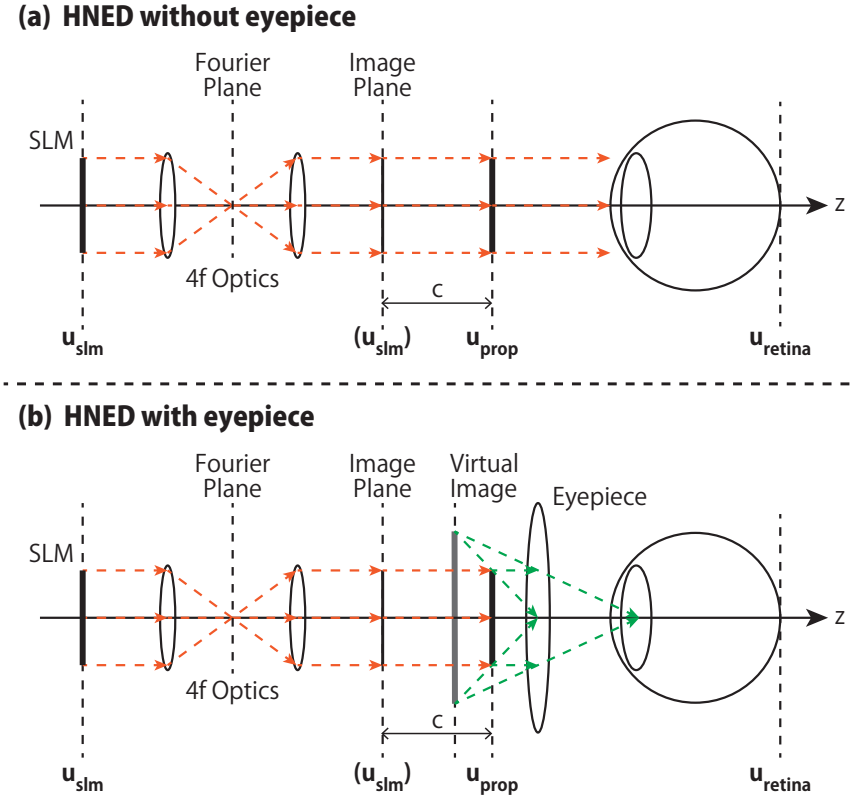

Figure 5.1: (a) Schematic diagram of HNED optical system without eyepiece. (b) Schematic diagram of the HNED optical system with eyepiece.

First, there is about HNED without eyepiece (Fig. 5.1(a)). In this optical system, the SLM plane is imaged on the image plane by the 4f optical system. Although the SLM image is flipped vertically and horizontally in the image plane, the phase distribution displayed on

SLM is reproduced as it is. The target object appears at a distance of c from the image plane. The user can see the object by observing this real image u_{prop}.

Next, HNED using an eyepiece is described (Fig. 5.1(b)). In this optical system as well, the SLM is imaged on the image plane by the 4f optical system and a real image u_{prop} is formed at a distance c from the image plane. The feature of this method is to observe this image using an eyepiece. Observing an image with an eyepiece is the same principle as magnifying an image with a magnifying glass. The observed image is a virtual image, and the position of the virtual image changes depending on the positional relationship between the real image and the eyepiece and the focal length of the eyepiece. The distance between the real image and the eyepiece must be less than the focal length of the eyepiece.

Each of these two methods has its advantages and disadvantages. The eyepiece-less approach results in an optical design similar to looking directly into the SLM. This approach can achieve the wide eyebox. However, the viewing angle depends on the diffraction limit of the SLM, and it is difficult to secure a sufficient viewing angle with the existing SLM pitch size. On the other hand, in the approach using the eyepiece, the real image is enlarged by the eyepiece, such that a considerably wide viewing angle can be realized. However, the use of eyepieces limits the position where the image can be observed, and the eyebox becomes smaller. In this way, there is a trade-off between the eyebox and the viewing angle between the two methods, and how to maximize both is still a research problem.

5.2 Calculating Phase Hologram on SLM

As shown in Fig. 5.1, while there are various methods for HNED, a standard optical design is existing. The point is that the target image or 3D object is reproduced by displaying the phase distribution on the phase SLM based on the hologram calculation. Calculating the phase distribution on the SLM is the essential part of the holographic display, and various methods have been proposed.

5.2.1 Iterative Fourier Transform Algorithm

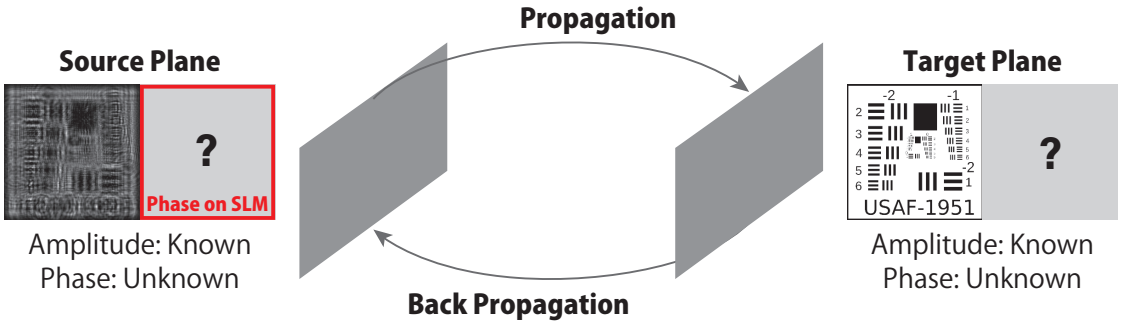

Figure 5.2: Schematic diagram of GS algorithm.

The most used method for calculating phase holograms is the Gerchberg-Saxton (GS) algorithm. This method was originally proposed as a phase retrieval method in 1972 [44]. As shown in Fig. 5.2, this is the method for searching the phase distribution when only the

amplitude value is known on the two planes. In the phase retrieval method, the phase is calculated using the image measured by the image sensor and the target image. In the phase calculation for hologram display, to derive the phase distribution to be displayed, the target image and the amplitude value after propagation are fixed, and the phase distribution to be displayed is optimized while the propagation is repeated. Various improved methods have been proposed based on this method; however, this thesis introduces only the original method.

5.2.2 Double Phase Amplitude Coding

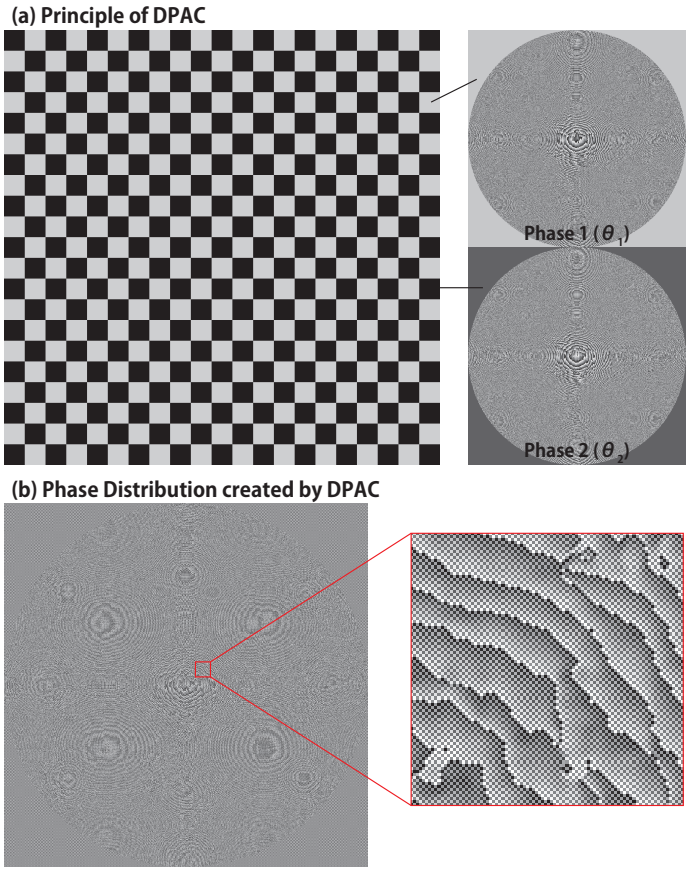

Figure 5.3: (a) Principle of DPAC method. Two phases are displayed in a checkerboard pattern. (b) Actual phase distribution created by DPAC method.

In image reproduction by hologram, it is generally known that the image reproduced from a hologram with complex amplitude (phase and amplitude) is reproduced more clearly than the image reproduced from a hologram with only amplitude or phase. However, in most cases, general SLM can only modulate either amplitude or phase. Therefore, research has been conducted to reproduce complex amplitude by adding some ingenuity to the optical system. In one famous approach, the principle was utilized to recover complex amplitude by adding two phases. The principle was proposed several decades ago [45] and can be

expressed by a mathematical formula as follows:

$$A\exp(i\theta) = \exp(i\theta_1) + \exp(i\theta_2) \tag{5.1}$$

$$\begin{cases} \theta_1 = \theta + \arccos(\frac{A}{2}) \\ \theta_2 = \theta - \arccos(\frac{A}{2}) \end{cases} \tag{5.2}$$

where $A\exp(i\theta)$ is the complex amplitude to be reproduced, A is the amplitude, and θ is the phase. The target complex amplitude is reproduced by two phases θ_1 and θ_2.

To utilize this principle, research has been conducted on phase or amplitude SLM using some technique. For example, it is a method of displaying two phase distributions on a single phase SLM and superimposing the two phase distributions utilizing a diffraction grating to recover complex amplitude [46, 47]. In this method, it is easy to superimpose two phases accurately; however, since two phase distributions must be displayed on a single SLM, the resolution is inevitably reduced. Besides, a method for recovering complex amplitude using two amplitude SLMs has also been proposed [48]. In this method, it is possible to avoid a decrease in resolution by using two SLMs; however, there are drawbacks such as the need for accuracy in adjusting the optical axis.

The double phase amplitude coding (DPAC) method proposed by Maimone et al. [2] addressed the problems of resolution reduction and optical axis adjustment. In this method, two phases are displayed in a checkerboard pattern, each equivalent to a single SLM (Fig. 5.3). This makes it possible to easily reproduce a complex amplitude distribution consisting of two phase distributions on a single SLM. However, since the checkered pattern is periodic, it is tended to generate diffracted light, and it has been pointed out that the amount of light decreases.

5.2.3 Solving Optimization Problem

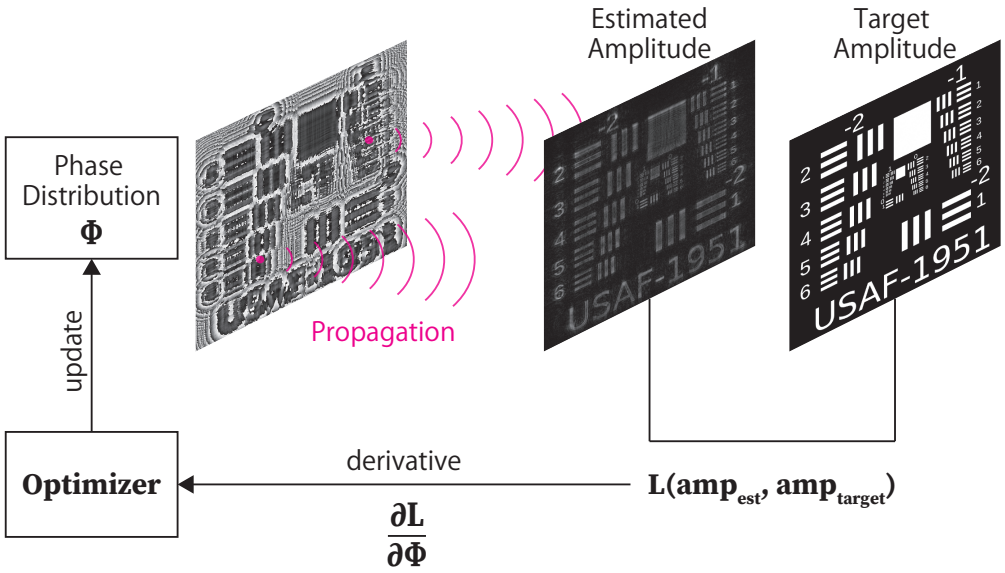

Figure 5.4: Workflow for optimizing phase holograms.

The GS algorithm has long existed as the primary method for calculating phase holograms; however, in recent years, the derivation of phase holograms has been treated as an optimiza-

tion problem. Figure 5.4 shows a schematic diagram of the phase hologram optimization problem. This is an optimization problem of finding the phase distribution ϕ that minimizes the difference between the target amplitude amp_{target} and the estimated amplitude amp_{est}. The formulation of this optimization problem is as follows:

$$\underset{\phi}{\text{minimize}}\ \mathcal{L}(amp_{est}, amp_{target}). \tag{5.3}$$

Recently, several optimization methods have been proposed to compute phase holograms on SLMs [49, 50, 51, 52]. In particular, it was demonstrated by Peng et al. [40] that automatic differentiation-based optimization is the best method for phase computation. However, it requires iterative processing, which is not suitable for fast processing, and should not be incorporated into interactive systems. Therefore, in this study, the DPAC method is adopted, which computes the phase hologram directly.

Chapter 6

Eye Aberration Correction

In this section, two methods of correcting eye aberrations in actual HNED are examined. One is a correction method that calculates the phase distribution reproduced in front of the eye with opposite aberration to the eye. The other is a method that calculates the shape of the observed image which is opposite to the image distortion caused by eye aberrations.

6.1 Solution 1: Inverse wavefront aberration

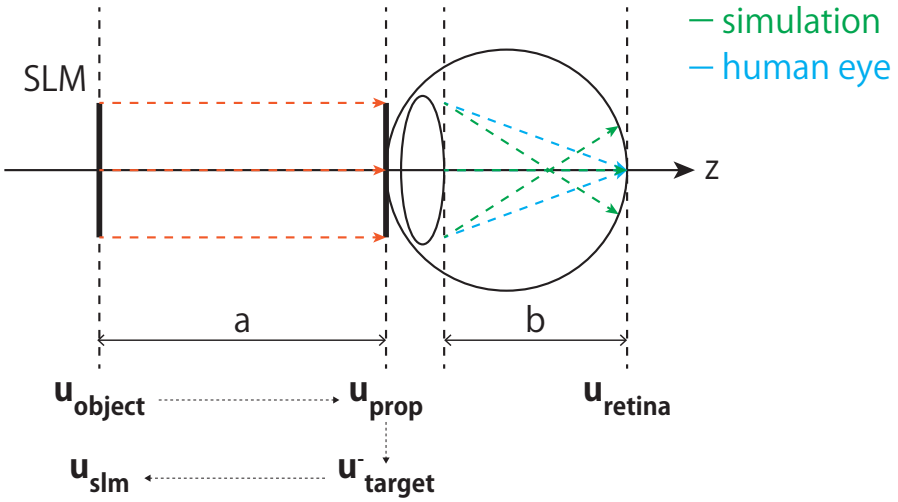

Figure 6.1: Schematic diagram of propagation in Solution 1.

The first method is to make the wavefront after passing through the lens with aberration the same as the wavefront after passing through the lens without aberration. This method utilizes the HNED optical system that does not use an eyepiece, as shown in Fig. 5.1(a). To achieve this method, the wavefront u^- in front of the lens should be reproduced with the aberration which is the opposite of the lens aberration. First, the generalized pupil function $\mathcal{P}_{rev}$ is calculated, which has the inverse aberration of the lens. Since the aberration of the lens is expressed by the wavefront aberration, when the aberration of the lens is $W(x, y)$, P_{rev} is expressed by the following equation:

$$\mathcal{P}_{rev}(x, y) = P(x, y) \exp(ik(-W(x, y))). \tag{6.1}$$

Second, the complex amplitude u^{-}_{target} is defined to be reproduced just before the lens as follows

$$u_{prop} = Prop_a(u_{object}) \tag{6.2}$$

$$u^{-}_{target} = u_{prop} * \mathcal{P}_{rev}(x, y). \tag{6.3}$$

Finally, to calculate the phase u_{slm} to be displayed on the SLM, u^{-}_{target} is backpropagated from the front of the lens to the SLM plane:

$$u_{slm} = Prop_{-a}(u^{-}_{target}). \tag{6.4}$$

The complex amplitude distribution obtained in this way, u_{slm}, is processed using the DPAC method to obtain the phase distribution displayed on the single SLM.
In the simulation, the propagation from the SLM plane to the retina is calculated. This formula is as follows:

$$u_{retina} = Prop_b(Prop_a(u_{slm}) * t(x, y) * \mathcal{P}(x, y)). \tag{6.5}$$

The simulation results of lens aberration correction using this method are shown in Fig. 6.2. In this simulation, vertical astigmatism is set as the lens aberration. It can be seen that by reproducing the reverse aberration in front of the lens, the aberration of the lens is canceled out and a clean image is formed.

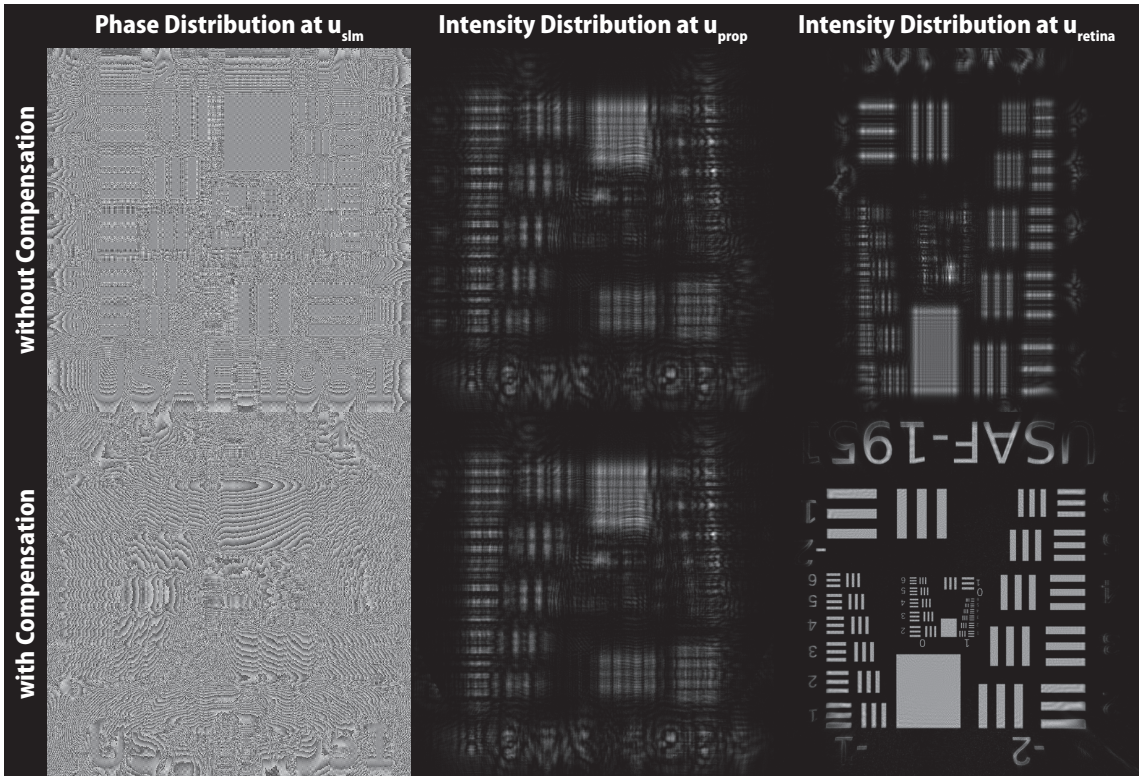

Figure 6.2: Simulation results of correcting vertical astigmatism in Solution 1.

However, there is a fatal problem with this method. The human eye cannot see the image directly (Fig. 6.1). This method is based on the premise that light propagates from plane to plane, and since collimated laser light is used, the light propagates in parallel. Although

it is easy to adjust the focus to an arbitrary position with a camera, the human eye cannot adjust. This method is implemented in an actual optical system and several people observed images through the setup. As a result, they could not observe the images like the simulation. Since the eye's focus adjustment is not possible, they could only see an image like a point light source (Fourier transformed image). Therefore, another method is needed that would allow human observation.

6.2 Solution 2: Inverse image shape

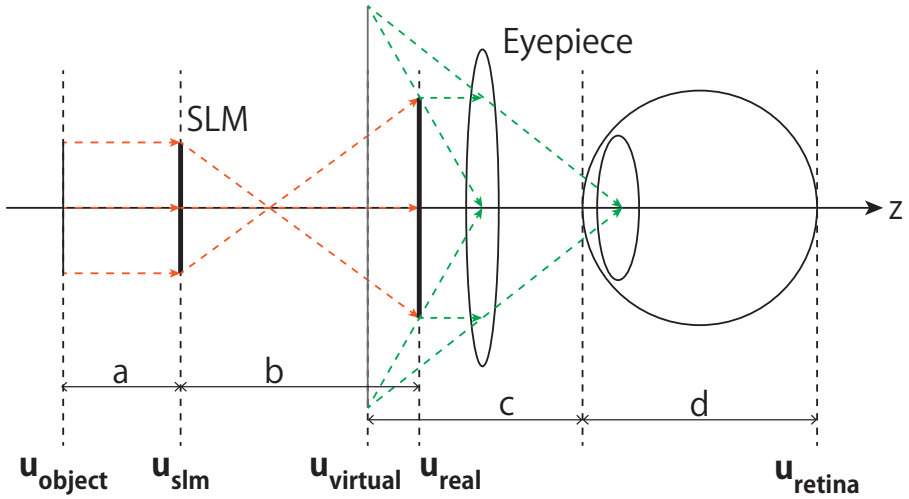

Figure 6.3: Schematic diagram of propagation in Solution 2.

Because Solution 1 became unobservable to humans, a human-observable optical system is designed. The main reason why the image could not be observed in Solution 1 is that the light incident on the eyes was parallel light. Therefore, HNED was designed using eyepieces (Fig. 5.1(b)). The aberration-correctable HNED system using an eyepiece is depicted in Fig. 6.3. In this optical system, the real image u_{real} is observed through an eyepiece. Because this optical system uses a virtual image, the imaging process with the wavefront propagation cannot be directly simulated. Therefore, the image magnification of the virtual image is ignored in simulations, and the image formed on the retina is calculated by treating the virtual image as the real image.

The real image observed through the eyepiece is calculated such that the distortion of the image is opposite to the distortion caused by the eye lens. The phase distribution to be displayed on the SLM is derived from the following propagation calculation:

$$u_{slm} = Prop_a(u_{object}) * t(x, y) * \mathcal{P}_{rev}(x, y) \tag{6.6}$$

where $\mathcal{P}_{rev}(x, y)$ contains aberrations that are the opposite of eye aberrations. The real image to be observed by the eyepiece can be obtained from the following propagation formula:

$$u_{real} = Prop_b(u_{slm}). \tag{6.7}$$

Only in the simulation, the real image is formed on the retina along with the following propagation formula:

$$u_{retina} = Prop_d(Prop_c(u_{real}) * t(x, y) * \mathcal{P}(x, y)). \tag{6.8}$$

The results of the simulation are presented in Fig. 6.4. In this simulation, corrections have been made for cases where the eyes have vertical or oblique astigmatism. As shown by these results, the aberration distortions can be corrected.

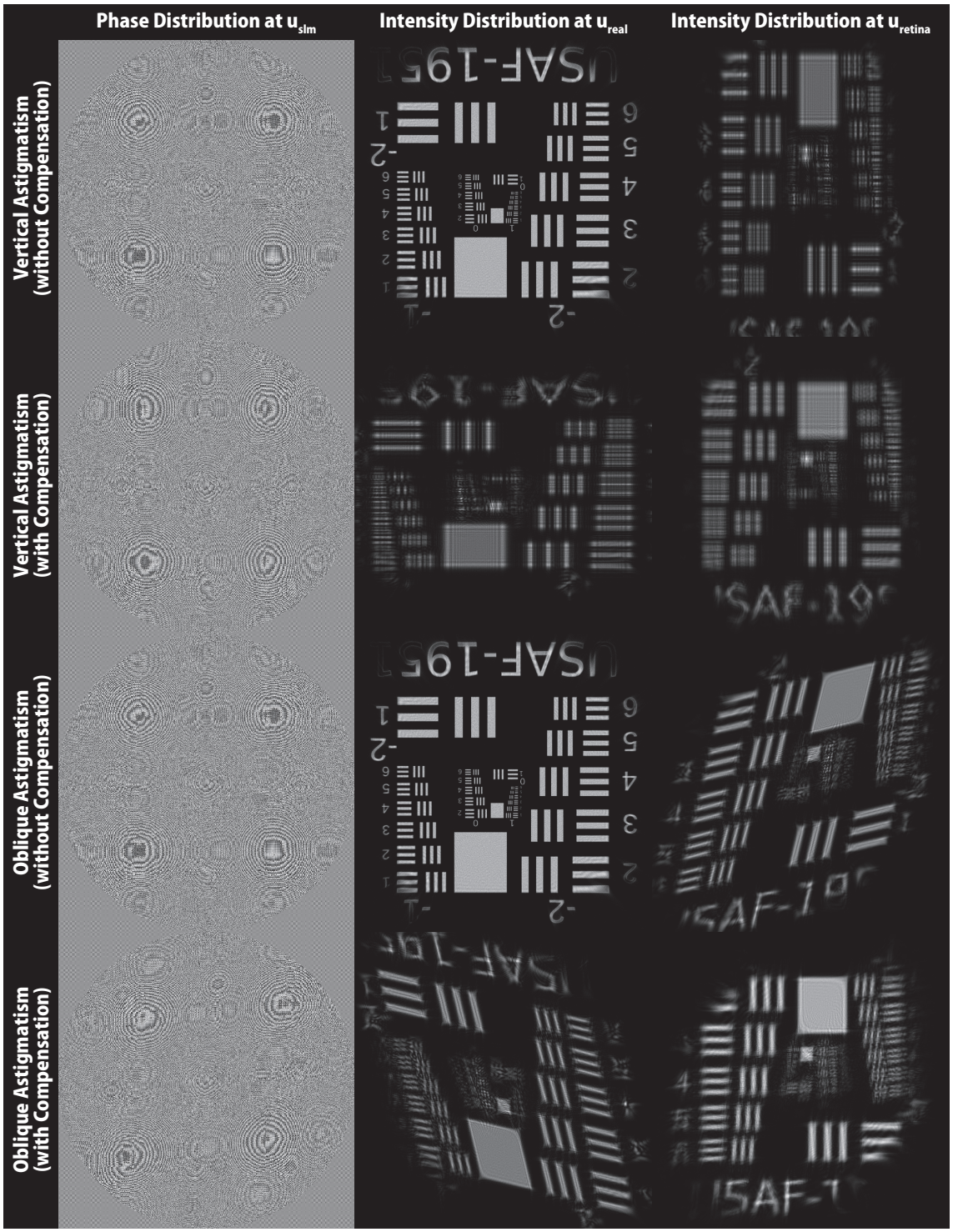

Figure 6.4: Simulation results of correcting vertical and oblique astigmatism in Solution 2.

Chapter 7

Result

In this section, an actual optical system is constructed based on the propagation formula proposed in Chapter 6 and present the results of the aberration correction.

7.1 Optical Setup

The setup of the optical system is depicted in Fig. 7.1. The light source was a 520 nm laser beam, which was collimated and then irradiated to the SLM through a linear polarizer. The SLM used in this experiment was Thorlabs Exulus-4K-1[1], with a pitch of 3.74 μm and a pixel count of 3840×2160. In this study, the central 2160×2160 pixels were used to display the phase distribution. The SLM depicts the phase distribution calculated using Eq. 6.6. Because the phase pattern displayed on the SLM included the lens pattern, the light modulated by the SLM was focused. Because the zeroth-order diffraction light was not included in the focused light, the aperture stop was set to cut off the zeroth-order light. Additionally, the first-order diffraction light from the SLM was used in this experiment because the amount of light coaxial to the optical axis was insufficient. The real image formed by the SLM lens pattern was observed using an eyepiece. The observed image was best seen when the position of the eyes was set at the focal length of the eyepiece. When reproducing aberration, an optical element (e.g., a cylindrical lens for astigmatism reproduction) was set at the position in front of the eye position.

[1] https://www.thorlabs.com/thorproduct.cfm?partnumber=EXULUS-4K1/M (last accessed Nov. 16, 2020)

7.2 Display Result

The change in the observed image with and without correction is depicted in Fig. 7.2. Images were taken with a camera (SONY ILCE-7RM2, 90 mm lens) in the position of the eyes. The aperture was open for all shots (f/2.8) and the camera was focused at a distance of 0.5 m. In Fig. 7.2, a ruler is attached to the image with no aberration as a reference size at 0.5 m. This experiment considered four types of astigmatism (horizontal, vertical, oblique, and mixed), myopia, and hyperopia. When reproducing horizontal, vertical, and oblique astigmatisms, one cylindrical lens (focal length of 100 mm) was set at an angle of 0°, 90°, and 45°, respectively. To reproduce myopia and hyperopia, plano-convex and plano-concave lenses with focal lengths of 100 mm and -100 mm, respectively, were used. Mixed astigmatism was reproduced by using two cylindrical lenses with two different focal lengths (100 mm and 150 mm) set at different angles.

For the sake of simplicity, the number of Zernike coefficients used in this experiment was reduced. For vertical and horizontal astigmatisms, the Zernike coefficient of $n, m = 2, 2$ was used; for oblique astigmatism, the Zernike coefficient of $n, m = 2, -2$ was used; for myopia and hyperopia, the Zernike coefficient of $n, m = 2, 0$ was used; and for mixed astigmatism, two Zernike coefficients of $n, m = 2, 2$ and $n, m = 2, -2$ were used (n, m are the same as those used in Eq. 3.11).

Four different images are prepared with uppercase E, USAF 1951, baboon, and checkerboard, and the results for each of the different aberration setting have been presented. In all cases, the image form was restored to an aberration-free state, indicating that the aberrations have been corrected.

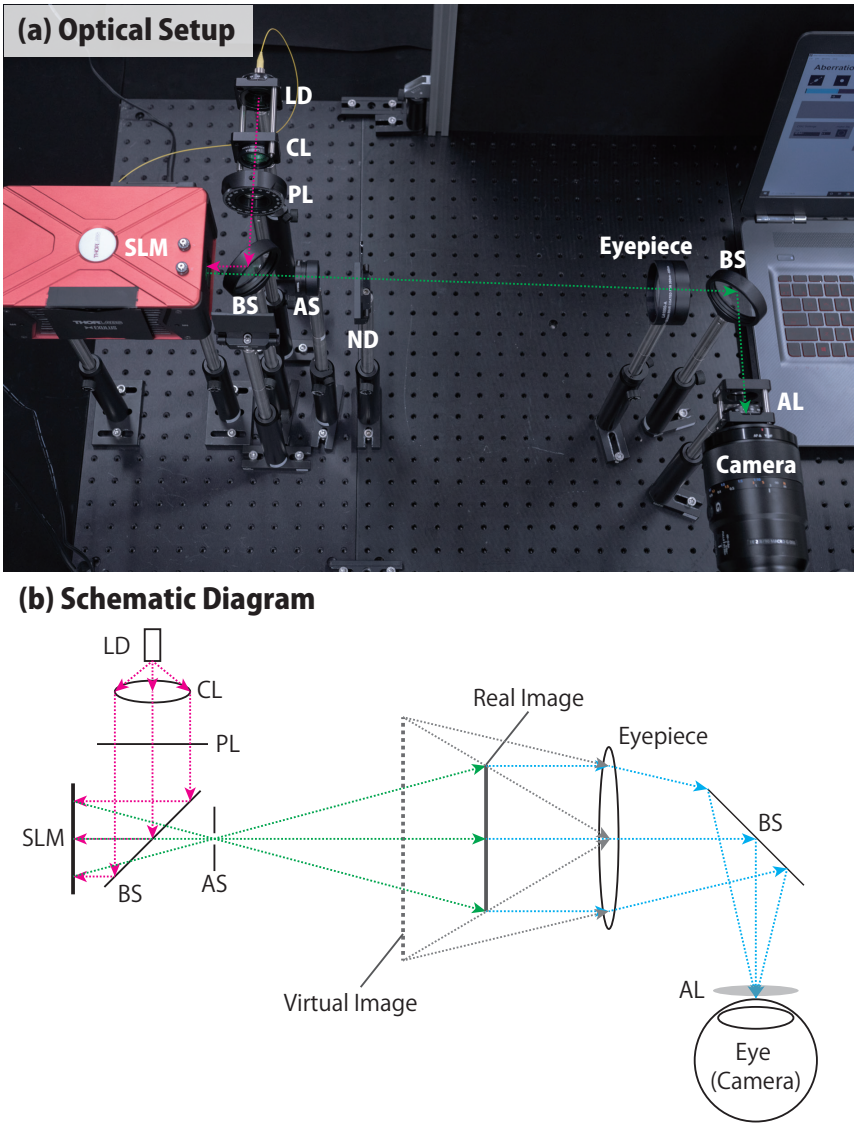

Figure 7.1: (a) Optical setup of the benchtop prototype of HNED. (b) Schematic of the optical setup. LD: laser diode; CL: collimator lens; PL: polarizer; BS: beam splitter; AS: aperture stop; ND: ND filter; AL: aberrated lens.

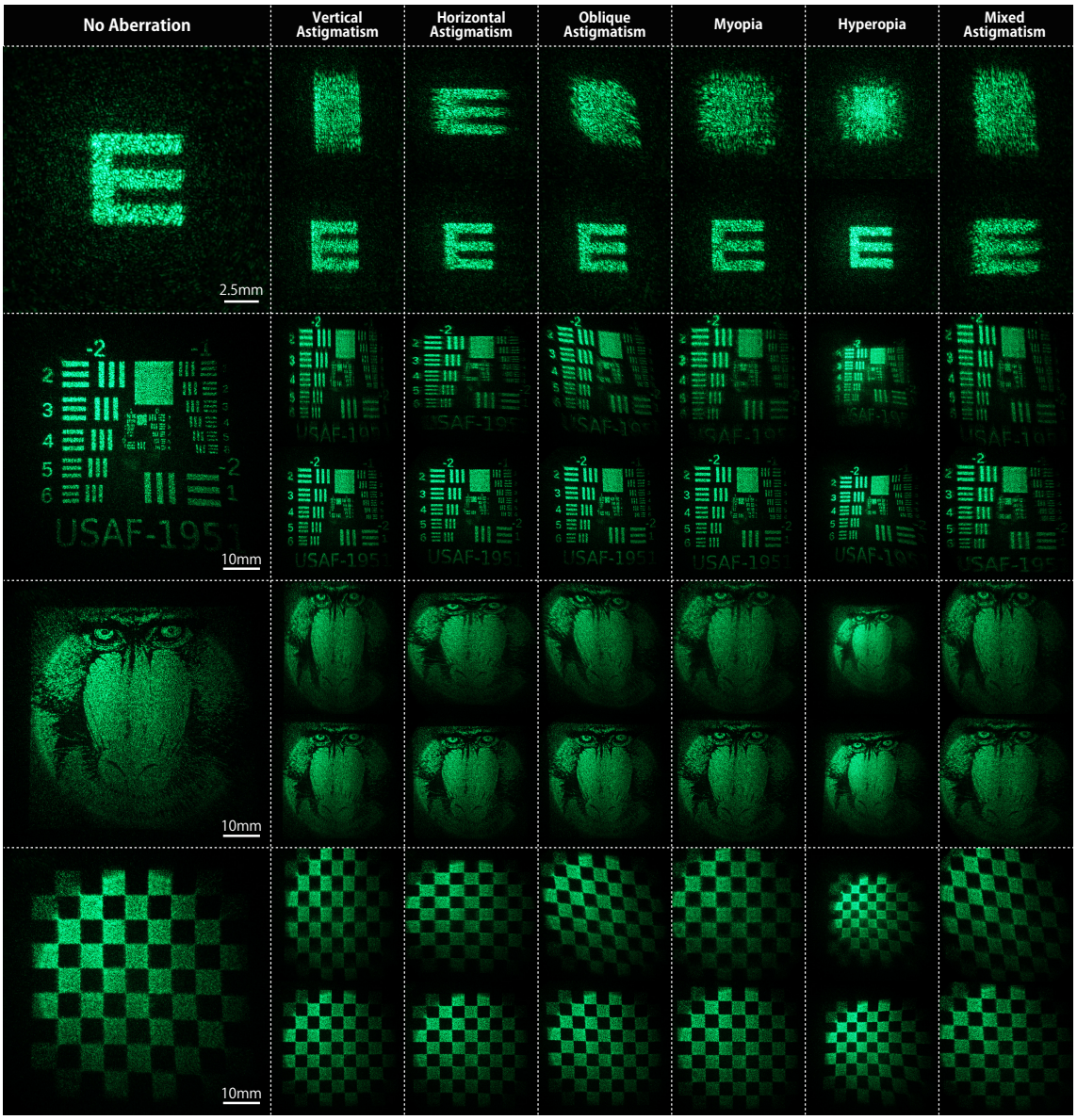

Figure 7.2: Display results by the HNED with and without aberration correction. Of each aberration correction result, the upper and lower column are the image before and after correction, respectively. There are six types of aberrations: horizontal astigmatism, vertical astigmatism, oblique astigmatism, myopia, hyperopia, and mixed astigmatism. In all aberration patterns, the displayed image can be compensated.

Chapter 8

User Interface and User Study

In the preceding sections, the optics of the near-eye display, aberration correction method, and display results are described. In this section, an interface is developed to enable users to adjust the correction coefficients on their own. Additionally, the experiment on humans is performed to analyze the results of the aberration correction using the proposed interface.

8.1 User Interface

In Section 5, the correction coefficients for each aberration were adjusted to demonstrate the correction results. The objective of providing a simple user interface is to enable the user to adjust the coefficients on their own.
Figure 8.1 (a) depicts the image of the experimental system and the user interface. The user interface is provided and the phase calculation is processed on the same computer. The SLM is connected to the computer via an HDMI cable. The user interface has a slide bar for adjusting each coefficient, as depicted in Fig. 8.1(b). In this experiment, for the sake of brevity, only correction coefficients corresponding to vertical and horizontal astigmatisms, oblique astigmatism, and myopia and hyperopia were used (although it is possible to provide coefficients for higher-order aberration corrections). The user can adjust the correction coefficients by moving the slide bar, and each time the coefficients are updated by pushing the button, a process is performed to calculate the phase distribution to be displayed on the SLM. The user can repeat the adjustment of the coefficients until the image is displayed correctly.

8.2 User Study

An experiment on human subjects is performed to validate the effectiveness of the proposed method. In this section, the summary and discussion about the design and results of the experiment is described.

8.2.1 Tasks

A visual acuity test-like task is set up to quantify the improvement in vision after correction. The letter E, also depicted in Fig. 7.2, is often used in visual acuity tests [53]. In a typical visual acuity test, participants are asked to name the direction letter E is pointing toward

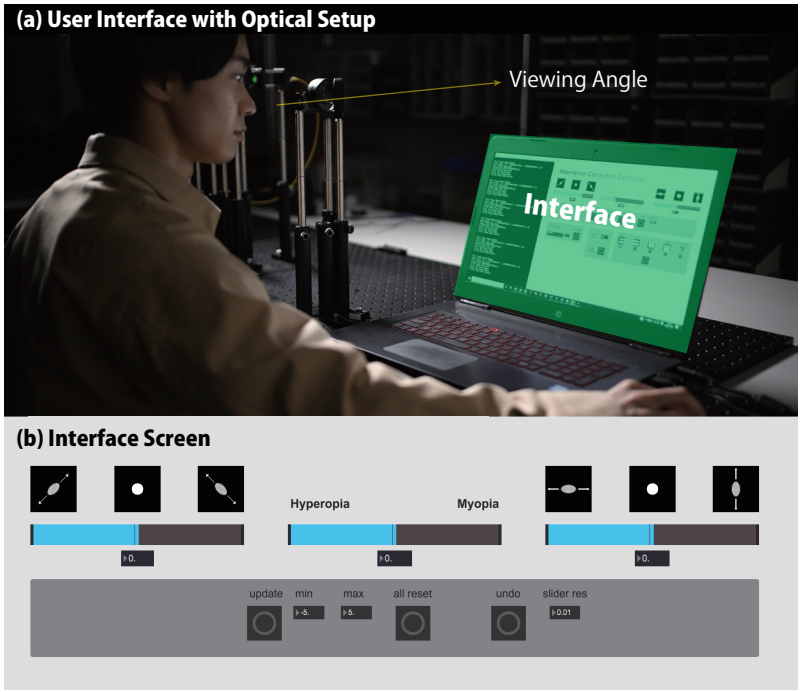

Figure 8.1: (a) Exterior view of the user's actual use of the interface with the HNED. (b) Screenshot of user interface used in this experiment. There are three slide bars and buttons for updating and resetting.

and their visual acuity is determined from their correct responses. In this experiment, whether the correction improved the participants' correct response rate is checked. The following four experimental conditions were set up.

1. Without aberration reproduction lens (participant's naked eyes only) and without correction by HNED.
2. Without aberration reproduction lens (participant's naked eyes only) and with correction by HNED.
3. With aberration reproduction lens and without correction by HNED.
4. With aberration reproduction lens and with correction by HNED.

Participants were asked to indicate the orientation (up, down, left, right) of letter E when they could recognize the letter. For the aberration reproduction lens, a cylindrical lens was used at a 45° angle to reproduce oblique astigmatism (same settings as shown in Fig. 7.2). It is noted that the size of the E letter when the direction of E as answered by the participant was correct. The magnitude of E was measured by the angle of view. It was assumed that 1 minute-angle (1/60°) at a distance of 5 m is equivalent to 1.454 mm, and the visual acuity of 1.0 corresponds to the visual acuity that can discriminate 1 minute-angle (Fig. 8.2). In this experiment, the minimum size to be displayed was 0.295° depending on the resolution of the display itself.

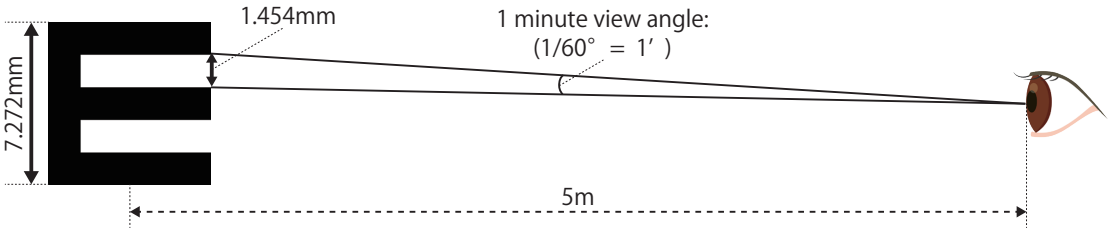

Figure 8.2: Relationship between viewing angle and E letter size and distance. When the observer can identify the equivalent of 1 minute-angle in the visual acuity test, the visual acuity is diagnosed as 1.0.

8.2.2 Procedure

Participants worked on the experiment in a room where the benchtop prototype of HNED was prepared. In the room where the experiment was conducted, the amount of light was slightly reduced such that the image displayed by the HNED could be easily seen. The participants first observed the sample image displayed by the HNED, confirmed which eye was easier to see, and decided which eye to use in the experiment. Next, they answered a pre-questionnaire about the eyes they used. After answering the questionnaire, they received an explanation of the experiment contents and how to use the user interface, and tried it to become familiar with the operation of the interface. The experiment was started when the participants were fully accustomed to the interface. The participants performed tasks 1 to 4 in sequence, and participants' answers and correction results were recorded. Since there were no restrictions on the number or time of trials for correction, the time used for the experiment was different for each participant; however each experiment time for all participants was within 30 minutes.

8.2.3 Participants

The participants were classified into two groups based on a pre-questionnaire. Group 1 (G1) comprised people who could manage their daily routines with their naked eyes, regardless of whether they owned glasses or contact lenses. There were nine participants (ages 20 to 26, mean 22.6±2.19) in this group, and their self-reported visual acuity had a mean of 1.056 and a standard deviation of 0.631. Group 2 (G2) comprised people who usually wore glasses and would be unable to manage their daily lives without them. There were nine participants (ages 20 to 24, mean 21.7±1.41) in this group , and their self-reported visual acuity had a mean of 0.154 and a standard deviation of 0.100. Of all participants, 12 were nearsighted, 1 participant was farsighted, and 6 participants were astigmatic. These two groups were tested under the four conditions described above.

8.2.4 Result

The boxplots for each group are depicted in Fig. 8.3 for the minimum size of the discriminable letter E measured under each experimental condition. The Wilcoxon rank sum test was used to analyze the experimental results before and after the correction with a significant difference of 5%. In G1, there were no significant difference between tasks 1 and 2 in the Wilcoxon rank sum test ($p = 0.1573$), because users with good eyesight could see

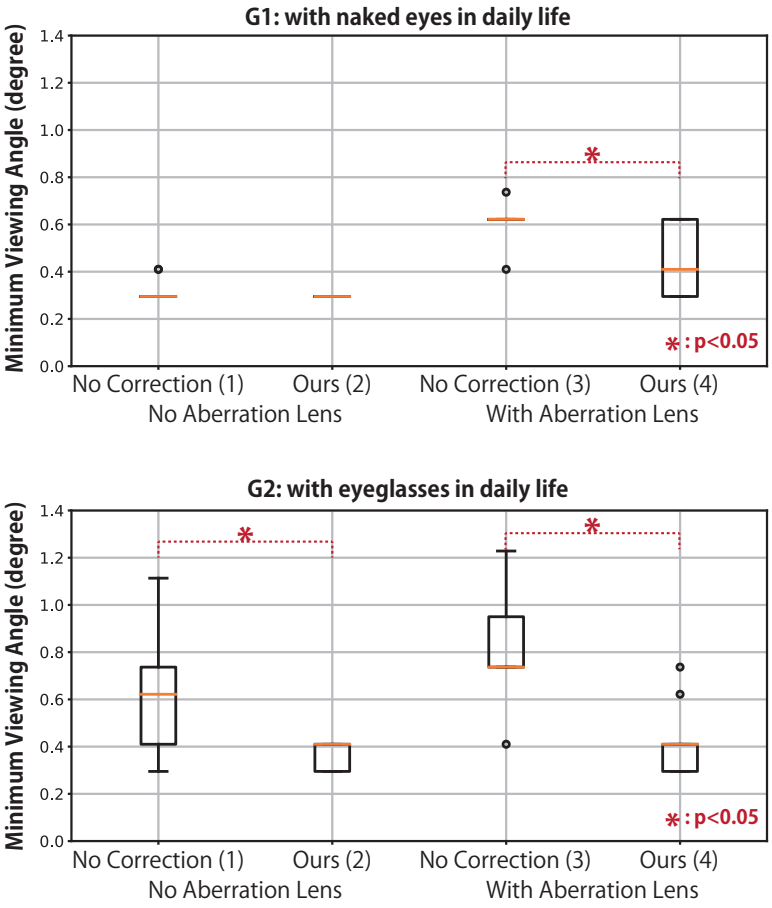

Figure 8.3: Boxplots of the results of the experiment. The orange line represents the median, box represents the quartile range, whiskers indicate minimum and maximum, and dots indicate the outliers.

the smallest size on the display, and there was no improvement from the correction. In contrast, an improvement between tasks 3 and 4 with the aberration reproduction lenses is recognized, with a significant difference in the Wilcoxon test ($p = 0.0412$). In G2, there was a significant difference between tasks 1 and 2 ($p = 0.0277$) and between tasks 3 and 4 ($p = 0.0112$).

These results indicate that the proposed correction interface is effective. In particular, the significant difference between tasks 1 and 2 in G2 is an important result that demonstrates the usefulness of the proposed method in correcting the visibility even for the user's naked eyes.

Chapter 9

Discussion

9.1 Optical Characteristics of Proposed HNED

9.1.1 Optical Limitations of HNED

As shown in Fig. 7.1, the HNED developed in this study is designed to observe the image formed by SLM through the eyepiece. It is considered that the minimum resolution of the HNED is slightly reduced due to the image formation by SLM and the image enlargement by the eyepiece. In the subject experiment in Chapter 8, the minimum viewing angle displayed by this HNED was 0.295° (17.7 arcmin angle). However, in a general visual acuity test, it is necessary to present a minimum viewing angle of about 0.017° (1 arcmin angle) in order to confirm a visual acuity of 1.0. Due to this lack of resolution, the accuracy of aberration correction has not been fully discussed.

In addition, in this HNED, the eyepiece was used to expand the viewing angle and human observability, which made the eyebox very narrow. To realize a practical HNED, it is required to have both a wide viewing angle and a large eyebox. In the optical system of this HNED, there is still room for improvement. In the future, when the eyebox is expanded (for example, a holographic optical element with multiple focal points is used for the eyepiece as in the previous research), it is necessary to precisely examine how effective the proposed aberration correction method is.

9.1.2 Image Distortion Independent of Focal Length

Many near-eye displays use eyepieces, and the optics that place the eye at the focus of the eyepiece are known as the Maxwellian view display or retinal display [54, 3, 55, 56]. The Maxwellian-type near-eye display has the advantage of displaying images independent of the focal length of the eye. By aligning the light path to the center of the pupil, the display is not affected by the eye. However, these displays are not completely free from eye aberrations. For example, Takaki et al. [3] demonstrated the need to consider the effect of astigmatism. In the experiments of this study, it is also found that people with severely impaired eyesight are affected by eye aberrations.

To investigate the relationship between the aberration and Maxwellian view in the optical system, the images at different focal positions are observed through an aberration reproduction lens (plano-convex lens with a focal length of 100 mm for myopia reproduction). Figure 9.1 depicts the results with and without an aberration reproduction lens. Under

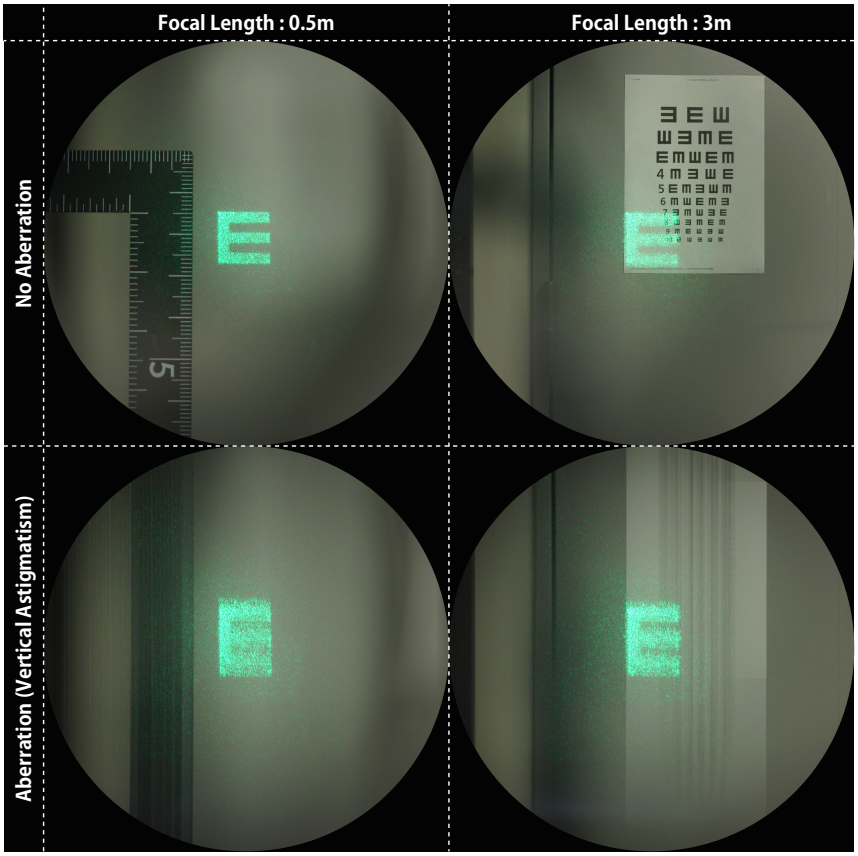

Figure 9.1: Images depicting the characteristics of the Maxwellian view. The upper and lower columns depict the images without and with an aberration-reproducing lens, respectively.

both conditions, the image does not depend on the focal length; in the presence of the aberration, the image is blurred even when the focal length is changed.
However, it is also true that the images produced by the Maxwellian view are not affected easily by aberrations. Therefore, although the proposed optical system is considered to be a Maxwellian-type near-eye display, the discussion of aberrations is essential.

9.1.3 Full-Color HNED

In this study, monochromatic aberrations are only focused on because one laser wavelength is only used for HNED. Colorization is an essential element in enriching HNED. Therefore, an experiment on aberration correction in full-color HNED is performed, taking pictures for each RGB wavelength and postprocessing them to simulate a full-color display. The exposure time of each image was 1/320 s, and images were displayed at 30 Hz on the SLM. The optical system used in the full-color experiment is depicted in Fig. 9.2(a). A laser combiner was used to unify the optical axes at all wavelengths, and a cylindrical lens with a focal length of 100 mm was used to reproduce the aberration.
Figure 9.2(b) depicts the results before and after the aberration correction. The same correction factors were used for aberration correction for all wavelengths. It is evident that aberration correction works even when the same correction factors are used. In the future, more detailed aberration correction will be required for each wavelength, and a higher frame

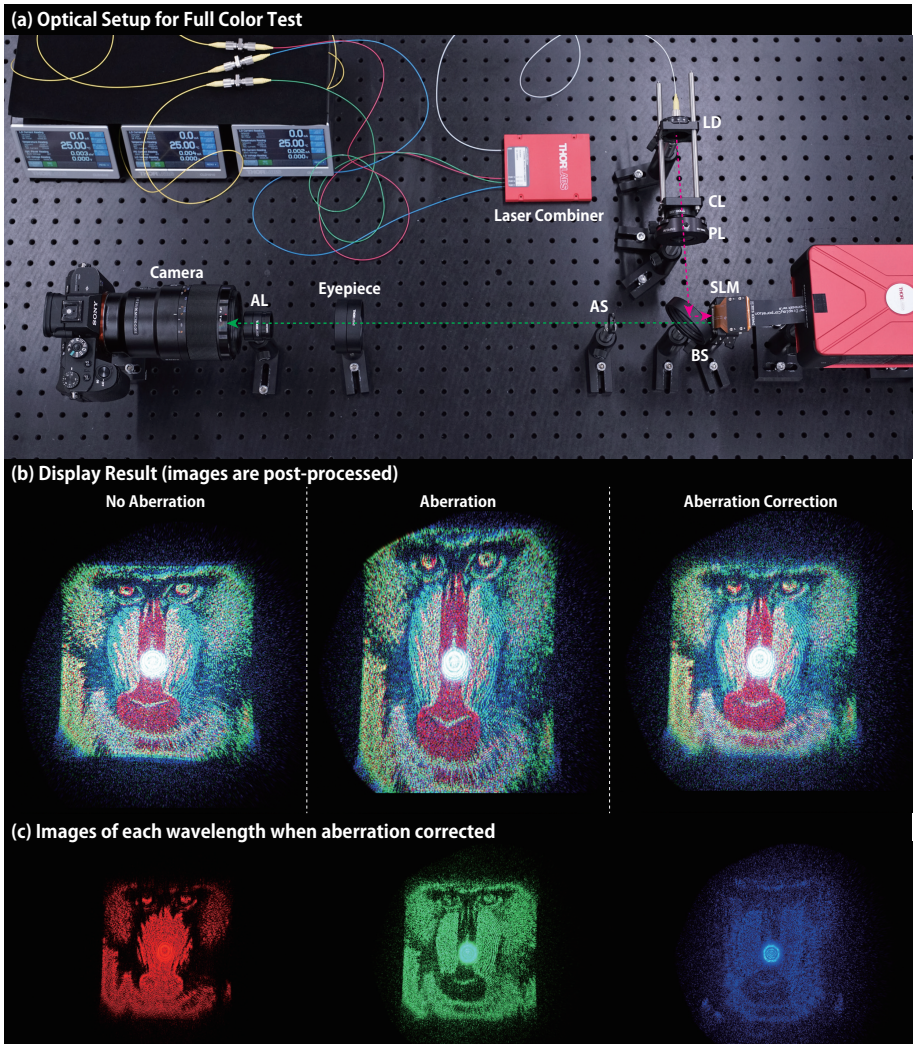

Figure 9.2: (a) An image of the optical system used in the full-color experiment. (b) Results of aberration correction in the full-color experiment. All images were post-processed from the images taken at each RGB wavelength.

rate of SLM will enable full-color observation.

9.1.4 Computer-Generated Hologram

The DPAC method was employed in this study to achieve a fast phase calculation. However, in principle, this method causes a reduction in the intensity of light [40]. In the DPAC method, a checkerboard pattern of phases on the SLM causes diffraction images and light dispersion. In the experiment by Peng et al. [40], the diffraction image was ignored and only the image generated coaxially with the optical axis was utilized. However, in the setup of this study, the amount of light in the image on the optical axis is extremely low owing to the use of the SLM with a smaller pitch size; hence, the diffracted image is only used.
To avoid these problems, a high-precision phase calculation method without a periodic structure is required. If interactive computation is required, it is necessary to perform the most appropriate phase computation based on the coefficient input by the user. Therefore, it is possible to build a neural network architecture with user-defined aberration correction

coefficients in the future.

9.1.5 Hardware Miniaturization

In this study, a lens pattern is added to the phase pattern displayed on the SLM for cutting the zeroth-order light. In this design, the distance from the SLM to the image plane is required, which increases the optical path length and enlarges the optical system. To realize spectacle-type devices for augmented reality in the future, it is necessary to optimize the phase distribution and make the optical design small. For example, if the phase distribution displayed on the SLM is close to the real image for the observation and the holographic optical element is placed at the position of the lens of the glasses as an eyepiece, miniaturization can be achieved.

9.2 Correction Adjustment Interface and User Study

The results in Section 8.2.4 demonstrate that aberration correction via the proposed interface was useful. However, further improvements to the proposed method and additional subject experiments are necessary.

9.2.1 Exploring Optimal Coefficients Values

The most important drawback is that the user may not be able to reach the appropriate coefficients in some cases. Although this interface allows users to adjust the coefficients by moving the slide bar freely, the search for the appropriate coefficients requires many trials. In the experiment, some users gave up adjusting the correction because the search was unsuccessful. The key to solving this problem is to make the search easy and accurate for users. The simplest method is to first move the slide bar slowly and automatically, and let the user select the most improved condition. If the user searches around the selected condition after making a selection, it is considered that accurate correction can be achieved without failing to correct the aberration. However, since a large number of combination patterns are presented to the user, this is a time-consuming method.
On the other hand, there are some pioneering works on this type of the optimization problem. These are the studies of treating an user as a black box or as a function that can answer only likes and dislikes, and inferring appropriate coefficients from the few responses [57, 58]. In the HNED, there can also be a method to search for coefficients by showing users some correction results and having them provide feedback on the quality of the adjustment results.

9.2.2 Hologram Calculation Time and Interactivity

As mentioned before, some people quit the search for the correction coefficient. This withdrawal may be due to the time required for a single attempt. In this experiment, the phase calculation to update the coefficients took approximately 4 s, and the coefficients had to be specified and then the update button is pressed to reflect the correction result. It is needed to reduce the calculation time to be able to see the result of the correction synchronized with the slide bar movement.

9.2.3 Lack of Human Subjects with Severe Astigmatism

In the subject experiment of this study, users with various eyesight participated. In particular, Section 8.2.4 revealed that the correction was effective for users with low eyesight. However, all users with low eyesight were myopia or hyperopia users. Since users with severe astigmatism were not recruited in the subject experiment, a lens that reproduces astigmatism was used in this experiment. In the future, it is necessary to experiment whether appropriate correction can be realized when a user with severe astigmatism actually uses this HNED.

Chapter 10

Conclusion

In this study, an HNED with an interactive aberration correction mechanism is proposed. A correction method for individual eye aberrations has not been studied thoroughly, and no studies have been conducted on the user interface for correction adjustment. To develop an HNED that can compensate for eye aberrations, light propagation including eyes with aberrations is formulated based on wave optics. In the proposed HNED, the phase including the aberration opposite to that of the eye is displayed by SLM. By propagating light from the SLM plane with inverse aberration to the image plane, a real image with distortion opposite to that of the eye can be obtained. This correction method was validated under the condition of reproducing eye aberrations with a spherical lens or a cylindrical lens, and it was verified that the correction was successful. Additionally, a GUI is developed that can work with the HNED to enable the user to make his or her own corrections because eye aberrations differ from individual to individual. This interface enables the user to search for the best coefficient values of aberration correction on their own. An experiment on human subjects is performed in which individuals with good and poor eyesight were invited to participate to validate the proposed method. As a subject experiment, an experiment such as a visual acuity test was performed. In this experiment, the minimum resolution that the user can identify before and after the correction was measured, and the improvement of the displayed image by the correction was quantitatively shown. Through the experiment, it is found that the aberration correction using the interface can help make images discriminable. In the future, some improvements and developments are required for aberration correction. Firstly, it will be necessary to propose a method to perform more detailed aberration correction that can handle higher-order aberrations. Secondly, it will be necessary to improve the correction method in order to reduce the burden on the user required for adjusting the correction. Finally, a method of aberration correction for other types of HNED will also be required. I believe that the formulation of the problem and proposed correction method will be useful for designing these aberration correction methods in the future.

Acknowledgement

I would like to show my greatest appreciation to Prof. Yoichi Ochiai. By spending a lot of time together, I learned a lot of important things from him as a researcher. I am very happy to be able to research with him. Ippei Suzuki, Kosaku Namikawa, and Kaisei Sato helped with the experimental design and interface development of this research, and I would like to thank them. Without their help, I would not have been able to submit a paper to an international conference. I would like to thank So Nishimura of Pixie Dust Technologies, Inc. for giving me regular feedback on this research from a technical point of view. CREST team members provided feedback on the research presentation in the early stage of this study. I also received feedback from many Pixie Dust Technologies, Inc. employees on the early demo of this study. I would like to express my appreciation to all of them. In addition, the members of Digital Nature Group have been supporting me not only in my research but also in my daily life. I appreciate it very much.
Finally, it was my family that greatly supported my current enjoyable research activities. I would like to express my deep gratitude to my family.

References

[1] Ivan E. Sutherland. A head-mounted three dimensional display. In *Proceedings of the December 9-11, 1968, Fall Joint Computer Conference, Part I*, AFIPS '68 (Fall, part I), page 757–764, New York, NY, USA, 1968. Association for Computing Machinery.

[2] Andrew Maimone, Andreas Georgiou, and Joel S. Kollin. Holographic near-eye displays for virtual and augmented reality. *ACM Trans. Graph.*, 36(4), July 2017.

[3] Yasuhiro Takaki and Naohiro Fujimoto. Flexible retinal image formation by holographic maxwellian-view display. *Opt. Express*, 26(18):22985–22999, Sep 2018.

[4] Dongyeon Kim, Kiseung Bang, Youngmo Jeong, and Byoungho Lee. Compensating high-order optical aberrations induced by abnormal shape of cornea in holographic displays. In *Frontiers in Optics + Laser Science APS/DLS*, page JW4A.102. Optical Society of America, 2019.

[5] Dongyeon Kim, Seung-Woo Nam, Kiseung Bang, and Byoungho Lee. P-81: Holographic near-to-eye display for vision-correcting application. *SID Symposium Digest of Technical Papers*, 51(1):1660–1663, 2020.

[6] Thomas Young. Ii. the bakerian lecture. on the mechanism of the eye. *Philosophical Transactions of the Royal Society of London*, (91):23–88, 1801.

[7] Gert Van den Brink. Measurements of the geometrical aberrations of the eye. *Vision Research*, 2(7-8):233–244, 1962.

[8] B Howland and HC Howland. Subjective measurement of high-order aberrations of the eye. *Science*, 193(4253):580–582, 1976.

[9] Howard C. Howland and Bradford Howland. A subjective method for the measurement of monochromatic∗ aberrations of the eye. *J. Opt. Soc. Am.*, 67(11):1508–1518, Nov 1977.

[10] Junzhong Liang, Bernhard Grimm, Stefan Goelz, and Josef F. Bille. Objective measurement of wave aberrations of the human eye with the use of a hartmann–shack wave-front sensor. *J. Opt. Soc. Am. A*, 11(7):1949–1957, Jul 1994.

[11] Heidi Hofer, Pablo Artal, Ben Singer, Juan Luis Aragón, and David R. Williams. Dynamics of the eye's wave aberration. *J. Opt. Soc. Am. A*, 18(3):497–506, Mar 2001.

[12] Jason Porter, Antonio Guirao, Ian G. Cox, and David R. Williams. Monochromatic aberrations of the human eye in a large population. *J. Opt. Soc. Am. A*, 18(8):1793–1803, Aug 2001.

[13] Junzhong Liang and David R. Williams. Aberrations and retinal image quality of the normal human eye. *J. Opt. Soc. Am. A*, 14(11):2873–2883, Nov 1997.

[14] Kevin M Tuohy. Contact lens, June 6 1950. US Patent 2,510,438.

[15] Douglas G Vanderlaan, Ivan M Nunez, Marcie Hargiss, Michele L Alton, and Susan Williams. Soft contact lenses, December 7 1999. US Patent 5,998,498.

[16] Paul C. Nicolson and Jürgen Vogt. Soft contact lens polymers: an evolution. *Biomaterials*, 22(24):3273 – 3283, 2001. Opthalmic Special Issue.

[17] Rafael Navarro, Esther Moreno-Barriuso, Salvador Bará, and Teresa Mancebo. Phase plates for wave-aberration compensation in the human eye. *Opt. Lett.*, 25(4):236–238, Feb 2000.

[18] Enrique J. Fernández, Ignacio Iglesias, and Pablo Artal. Closed-loop adaptive optics in the human eye. *Opt. Lett.*, 26(10):746–748, May 2001.

[19] Yuta Itoh and Gudrun Klinker. Vision enhancement: Defocus correction via optical see-through head-mounted displays. In *Proceedings of the 6th Augmented Human International Conference*, AH '15, page 1–8, New York, NY, USA, 2015. Association for Computing Machinery.

[20] David J. Apple, Nick Mamalis, Katherine Loftfield, Joseph M. Googe, Linda C. Novak, Dolores Kavka-Van Norman, Steven E. Brady, and Randall J. Olson. Complications of intraocular lenses. a historical and histopathological review. *Survey of Ophthalmology*, 29(1):1 – 54, 1984.

[21] David J. Apple, Kerry D. Solomon, Manfred R. Tetz, Ehud I. Assia, Elizabeth Y. Holland, Ulrich F.C. Legler, Julie C. Tsai, Victoria E. Castaneda, Judy P. Hoggatt, and Alexandra M.P. Kostick. Posterior capsule opacification. *Survey of Ophthalmology*, 37(2):73 – 116, 1992.

[22] Samir A Melki and Dimitri T Azar. Lasik complications: Etiology, management, and prevention. *Survey of Ophthalmology*, 46(2):95 – 116, 2001.

[23] Andrew B. Watson. Computing human optical point spread functions. *Journal of Vision*, 15(2):26–26, 02 2015.

[24] Steven A. Cholewiak, Gordon D. Love, and Martin S. Banks. Creating correct blur and its effect on accommodation. *Journal of Vision*, 18(9):1–1, 09 2018.

[25] Brian A. Barsky. Vision-realistic rendering: Simulation of the scanned foveal image from wavefront data of human subjects. In *Proceedings of the 1st Symposium on Applied Perception in Graphics and Visualization*, APGV '04, page 73–81, New York, NY, USA, 2004. Association for Computing Machinery.

[26] Matthias Nießner, Roman Sturm, and Günther Greiner. Real-time simulation and visualization of human vision through eyeglasses on the gpu. In *Proceedings of the 11th ACM SIGGRAPH International Conference on Virtual-Reality Continuum and its Applications in Industry*, pages 195–202, 2012.

[27] Masanori Kakimoto, Tomoaki Tatsukawa, Yukiteru Mukai, and Tomoyuki Nishita. Interactive simulation of the human eye depth of field and its correction by spectacle lenses. *Computer Graphics Forum*, 26(3):627–636, 2007.

[28] Steven A. Cholewiak, Gordon D. Love, Pratul P. Srinivasan, Ren Ng, and Martin S. Banks. Chromablur: Rendering chromatic eye aberration improves accommodation and realism. *ACM Trans. Graph.*, 36(6), November 2017.

[29] Enrique Josua Fernández. Adaptive optics for visual simulation. *International Scholarly Research Notices*, 2012, 2012.

[30] Carmen Cánovas, Pedro M. Prieto, Silvestre Manzanera, Alejandro Mira, and Pablo Artal. Hybrid adaptive-optics visual simulator. *Opt. Lett.*, 35(2):196–198, Jan 2010.

[31] Nikolai Suchkov, Enrique J. Fernández, and Pablo Artal. Wide-range adaptive optics visual simulator with a tunable lens. *J. Opt. Soc. Am. A*, 36(5):722–730, May 2019.

[32] Fu-Chung Huang and Brian A. Barsky. A framework for aberration compensated displays. Technical Report UCB/EECS-2011-162, EECS Department, University of California, Berkeley, Dec 2011.

[33] Fu-Chung Huang, Douglas Lanman, Brian A. Barsky, and Ramesh Raskar. Correcting for optical aberrations using multilayer displays. *ACM Trans. Graph.*, 31(6), November 2012.

[34] Vitor F. Pamplona, Manuel M. Oliveira, Daniel G. Aliaga, and Ramesh Raskar. Tailored displays to compensate for visual aberrations. *ACM Trans. Graph.*, 31(4), July 2012.

[35] Fu-Chung Huang, Gordon Wetzstein, Brian A. Barsky, and Ramesh Raskar. Eyeglasses-free display: Towards correcting visual aberrations with computational light field displays. *ACM Trans. Graph.*, 33(4), July 2014.

[36] Han-Ju Yeom, Hee-Jae Kim, Seong-Bok Kim, HuiJun Zhang, BoNi Li, Yeong-Min Ji, Sang-Hoo Kim, and Jae-Hyeung Park. 3d holographic head mounted display using holographic optical elements with astigmatism aberration compensation. *Opt. Express*, 23(25):32025–32034, Dec 2015.

[37] Wen-Kai Lin, Osamu Matoba, Bor-Shyh Lin, and Wei-Chia Su. Astigmatism and deformation correction for a holographic head-mounted display with a wedge-shaped holographic waveguide. *Appl. Opt.*, 57(25):7094–7101, Sep 2018.

[38] Jin Su Lee, Yoo Kwang Kim, and Yong Hyub Won. See-through display combined with holographic display and maxwellian display using switchable holographic optical element based on liquid lens. *Opt. Express*, 26(15):19341–19355, Jul 2018.

[39] Seung-Woo Nam, Seokil Moon, Byounghyo Lee, Dongyeon Kim, Seungjae Lee, Chang-Kun Lee, and Byoungho Lee. Aberration-corrected full-color holographic augmented reality near-eye display using a pancharatnam-berry phase lens. *Opt. Express*, 28(21):30836–30850, Oct 2020.

[40] Yifan Peng, Suyeon Choi, Nitish Padmanaban, and Gordon Wetzstein. Neural Holography with Camera-in-the-loop Training. *ACM Trans. Graph. (SIGGRAPH Asia)*, 2020.

[41] Praneeth Chakravarthula, Ethan Tseng, Tarun Srivastava, Henry Fuchs, and Felix Heide. Learned hardware-in-the-loop phase retrieval for holographic near-eye displays. *ACM Transactions on Graphics (TOG)*, 39(6):186, 2020.

[42] G. Tricoles. Computer generated holograms: an historical review. *Appl. Opt.*, 26(20):4351–4360, Oct 1987.

[43] Fernando Diaz-Douton, Antonio Benito, Jaume Pujol, Montserrat Arjona, Jose Luis Guell, and Pablo Artal. Comparison of the Retinal Image Quality with a Hartmann-Shack Wavefront Sensor and a Double-Pass Instrument. *Investigative Ophthalmology Visual Science*, 47(4):1710–1716, 04 2006.

[44] Ralph W Gerchberg. A practical algorithm for the determination of phase from image and diffraction plane pictures. *Optik*, 35:237–246, 1972.

[45] C. K. Hsueh and A. A. Sawchuk. Computer-generated double-phase holograms. *Appl. Opt.*, 17(24):3874–3883, Dec 1978.

[46] Jung-Ping Liu, Wang-Yu Hsieh, Ting-Chung Poon, and Peter Tsang. Complex fresnel hologram display using a single slm. *Appl. Opt.*, 50(34):H128–H135, Dec 2011.

[47] Qiankun Gao, Juan Liu, Xinhui Duan, Tao Zhao, Xin Li, and Peilin Liu. Compact see-through 3d head-mounted display based on wavefront modulation with holographic grating filter. *Opt. Express*, 25(7):8412–8424, Apr 2017.

[48] Qiankun Gao, Juan Liu, Jian Han, and Xin Li. Monocular 3d see-through head-mounted display via complex amplitude modulation. *Opt. Express*, 24(15):17372–17383, Jul 2016.

[49] Jingzhao Zhang, Nicolas Pégard, Jingshan Zhong, Hillel Adesnik, and Laura Waller. 3d computer-generated holography by non-convex optimization. *Optica*, 4(10):1306–1313, Oct 2017.

[50] Praneeth Chakravarthula, Yifan Peng, Joel Kollin, Henry Fuchs, and Felix Heide. Wirtinger holography for near-eye displays. *ACM Trans. Graph.*, 38(6), November 2019.

[51] Grace Kuo, Laura Waller, Ren Ng, and Andrew Maimone. High resolution étendue expansion for holographic displays. *ACM Trans. Graph.*, 39(4), July 2020.

[52] Praneeth Chakravarthula, Ethan Tseng, Tarun Srivastava, Henry Fuchs, and Felix Heide. Learned hardware-in-the-loop phase retrieval for holographic near-eye displays. *ACM Trans. Graph.*, 39(6), November 2020.

[53] J. E. Lovie-Kitchin. Validity and reliability of visual acuity measurements. *Ophthalmic and Physiological Optics*, 8(4):363–370, 1988.

[54] Mitsuru Sugawara, Makoto Suzuki, and Nori Miyauchi. 14-5l: Late-news paper: Retinal imaging laser eyewear with focus-free and augmented reality. *SID Symposium Digest of Technical Papers*, 47(1):164–167, 2016.

[55] Changwon Jang, Kiseung Bang, Seokil Moon, Jonghyun Kim, Seungjae Lee, and Byoungho Lee. Retinal 3d: Augmented reality near-eye display via pupil-tracked light field projection on retina. *ACM Trans. Graph.*, 36(6), November 2017.

[56] Seong-Bok Kim and Jae-Hyeung Park. Optical see-through maxwellian near-to-eye display with an enlarged eyebox. *Opt. Lett.*, 43(4):767–770, Feb 2018.

[57] Brochu Eric, Nando Freitas, and Abhijeet Ghosh. Active preference learning with discrete choice data. In J. Platt, D. Koller, Y. Singer, and S. Roweis, editors, *Advances in Neural Information Processing Systems*, volume 20, pages 409–416. Curran Associates, Inc., 2008.

[58] Yuki Koyama, Issei Sato, and Masataka Goto. Sequential gallery for interactive visual design optimization. *ACM Trans. Graph.*, 39(4), July 2020.